Colloid Polym Sci (2004) 282: 357–365
DOI 10.1007/s00396-003-0945-7

ORIGINAL CONTRIBUTION

Datchanee Chotpattananont
Anuvat Sirivat
Alexander M. Jamieson

Electrorheological properties of perchloric acid-doped polythiophene suspensions

Received: 17 February 2003
Accepted: 22 May 2003
Published online: 6 August 2003

D. Chotpattananont · A. Sirivat (✉)
The Petroleum and Petrochemical College,
Chulalongkorn University,
10330 Bangkok, Thailand
E-mail: anuvat.s@chula.ac.th

A. M. Jamieson
Department of Macromolecular Science
and Engineering, Case Western Reserve
University, Cleveland, OH 44106-7202,
USA

Abstract Poly(3-thiopheneacetic acid), PTAA, was synthesized via an oxidative polymerization and doped with perchloric acid to control its conductivity. The rheological properties of the $HClO_4$-doped PTAA/silicone oil suspensions were measured in oscillatory shear to investigate the effects of electric field strength, particle concentration, and particle conductivity on electrorheological (ER) characteristics. The PTAA-based ER fluids exhibit viscoelastic behavior under an applied electric field and the ER response is amplified with increase of electric field strength. The dynamic moduli, G' and G'', increase dramatically by ten orders of magnitude when the field strength is increased to 2 kV/mm. The suspensions exhibit a transition from fluid-like to solid-like behavior as the field strength increases, and reach a saturated ER response at a field strength of 1 kV/mm. Increase of particle concentration and particle conductivity result in a lower transition field strength. Scaling arguments are presented which successfully superpose the scaled moduli at various electric field strengths onto a single master function of the dimensionless frequency.

Keywords Electrorheological fluid · Conductive polymer · Polythiophene · Perchloric acid

Introduction

Electrorheological (ER) fluids are suspensions that exhibit a dramatic change in rheological properties in the presence of AC or DC electric fields. Commonly, they are composed of polarizable particles dispersed in a nonconducting fluid. On application of an electric field, chain-like or fibrillar aggregates of the suspended particles are oriented along the direction of the electric field, thereby inducing viscoelasticity and a drastic increase in viscosity [1]. The ability of these materials to transform electrical energy into mechanical energy has motivated research and development into various technological applications, as the active elements of clutches, brakes, shock absorbers, engine mounts, valves, and flow pumps [2, 3, 4, 5]. Typically, the steady-state rheological properties have been investigated for most ER fluids. The dynamic rheological responses, which probe the equilibrium structure of these materials in the presence and absence of the applied field, have not been studied so extensively [6, 7, 8, 9, 10].

Recently, there has been interest in using conductive polymers as suspended particles for dry-base ER fluids. Conductive polymers can offer a variety of advantages for ER systems: better thermal stability, insolubility, and more controllable viscosity. Suspensions of conductive polymers exhibit intrinsic ER properties without the necessity to introduce other additives. The polarization is induced by the motion of electrons within the suspended particles under application of an electric field. Various conductive polymers have been tested as particulate materials in ER systems. Examples include polyaniline (PANI) and its derivatives [11, 12, 13, 14, 15], PANI copolymers [16, 17, 18, 19], polypyrrole [20, 21], poly(acene quinone) radicals [19], poly(naphthalene quinone) radicals [22], and poly(*p*-phenylene) [19, 23].

In this study, we explore the ER behavior of poly(3-thiopheneacetic acid) (PTAA), doped with perchloric acid ($HClO_4$) to vary the conductivity. The dynamic moduli of $HClO_4$-doped PTAA suspensions were investigated in the presence and absence of applied electric fields. The effect of field strength, mechanical deformation frequency, doping degree (conductivity values), and particle concentration on the moduli were investigated and compared with existing theory.

Experimental

Materials

3-Thiopheneacetic acid, 3TAA (AR grade, Fluka), was used as the monomer. Anhydrous ferric chloride, $FeCl_3$ (AR grade, Riedel-de Haen), was used as the oxidant. Chloroform, $CHCl_3$ (AR grade, Lab-Scan), and methanol, CH_3OH (AR grade, Lab-Scan), were dried over CaH_2 for 24 h under a nitrogen atmosphere and then distilled. The perchloric acid dopant, $HClO_4$ (AR grade, AnalaR), was used as received. The dispersing phase was silicone oil (AR grade, Dow Corning) with density 0.96 g/cm^3 and kinematic viscosity 100 cSt, and was vacuum dried and stored in a desiccator prior to use.

Polymerization procedure

PTAA was synthesized by oxidative-coupling polymerization according to the method of Kim et al. [24]. 3TAA (10.0 g) was refluxed for 24 h in 50 ml of dry methanol with 1 drop of concentrated H_2SO_4, to protect against the oxidative decomposition of the carboxylic acid group of the monomer during polymerization. The methanol was evaporated and the residue was extracted with diethyl ether. The extract was washed with deionized water, dried with anhydrous $MgSO_4$, and then filtered. The diethyl ether was evaporated from the filtrate by a rotating evaporator.

A solution of 10 mmol of protected monomer in 20 ml chloroform was added dropwise to a solution of 40 mmol ferric chloride in 30 ml chloroform under a nitrogen atmosphere. The reaction was carefully maintained at 0 °C (±0.5 °C) for 24 h. The reaction mixture was precipitated by pouring into a large excess of methanol. The precipitate was repeatedly washed with methanol and deionized water. The precipitate was hydrolyzed by heating 0.5 g precipitate in 50 ml of 2.0 M NaOH solution for 24 h at 100 °C. The PTAA obtained was neutralized and precipitated with a dilute HCl solution. The PTAA was washed several times with deionized water before vacuum drying at room temperature for 2 days.

To examine the effect of particle conductivity on the electrorheological properties, PTAA particles having different conductivity values were prepared by doping with perchloric acid [25]. The $HClO_4$-doped PTAA was prepared by stirring ground PTAA (~7.04 mmol) with $HClO_4$ aqueous solution at room temperature for 3 days. The amounts of acid used were 7.04 ml of ~0.1 M aqueous acid and 176 ml of ~4.0 M aqueous acid for low and high doping ratios of 1.09×10^{-3} and 0.255, respectively. The $HClO_4$-doped PTAA particles were filtered and vacuum dried for 24 h before grinding with a mortar and pestle and then passed through a 38-μm sieve shaker to control the particle size distribution.

Preparation of ER fluids

The ER fluids were prepared by dispersing $HClO_4$-doped PTAA particles in silicone oil (density 0.96 g/cm^3 and kinematic viscosity 100 cSt) with an ultrasonicator for 30 min at 25 °C. The prepared ER fluids were then stored in a desiccator prior to use and redispersed before each measurement.

Characterization methods

Fourier-transform infrared (FT-IR) spectra were obtained using a FT-IR spectrometer (Bruker, Equinox 55/FRA 1065) operated in the transmission mode with 32 scans and a resolution of ±4 cm^{-1}, covering a wavenumber range of 4000–400 cm^{-1} using a deuterated triglycine sulfate detector. Optical grade KBr (Carlo Erba Reagent) was used as the background material. The synthesized PTAA was intimately mixed with dried KBr at a ratio of PTAA:KBr = 1:20.

^{1}H-NMR spectra in the solution state were recorded at 25 ± 1 °C using a 300 MHz digital NMR spectrometer (Bruker, DPX-300). Deuterated dimethyl sulfoxide was used as the standard solvent.

The UV-visible (UV-Vis) spectrum of the synthesized PTAA powder, dissolved in DMSO, was recorded with a UV-Vis spectrometer (Perkin Elmer, Lambda 10) at a scan speed of 240 mm/min and a slit width of 2.0 nm, using a deuterium lamp as the light source, at wavelengths between 190 and 800 nm.

The thermal stability of PTAA was investigated using a thermogravimetric analyzer (Perkin Elmer, TGA7) in the temperature range 25–750 °C at a heating rate of 10 °C/min.

The particle size distribution of PTAA powder was determined using a particle size analyzer (Malvern, Master Sizer X).

Scanning electron micrographs were taken with a scanning electron microscope (JEOL, JSM-5200-2AE) using an acceleration voltage of 20 kV and a magnification of 1,000.

To determine the electrical conductivity, $HClO_4$-doped polythiophene disks (25 mm diameter and ~0.2 mm thickness) were prepared by molding with a hydraulic press. Electrical conductivity was measured using a custom-built four-point probe. The specific conductivity, σ (S/cm), was obtained by measuring the resistance, R, and using the following relation: $\sigma = (1/Rt)(1/K)$, where t is the film thickness and K is the geometric correction factor. A geometric correlation factor was calibrated by using standard silicon wafer sheets with known specific resistivity values. The measurements were performed in the linear Ohmic regime, i.e., the specific conductivity values were independent of the applied DC current. The measurements were carried out at 27 °C and repeated at least two times.

A fluids rheometer (Rheometrics, ARES) was used to investigate the rheological properties. It is fitted with a custom-built copper parallel plates fixture (25 mm diameter) attached to insulating plexiglass sheets. A DC voltage was applied with a DC power supply (Tektronic, PS280) and a custom-built DC power supply, which can deliver an electric field strength to 2 kV/mm. A digital multimeter (Tektronic, CDM 250) was used to monitor voltage and current.

When evaluating the steady-state ER response, the electric field was applied for 10 min to ensure formation of an equilibrium agglomerate structure before measurements were taken. Each measurement was carried out at a temperature of 25 ± 0.1 °C and repeated at least two or three times.

In these experiments, G′ and G″ were determined as a function of frequency and electric field strength. Strain sweep tests were first carried out to determine the strain appropriate to measure G′ and G″ in the linear viscoelastic regime. The appropriate strain was determined to be 0.1% for electric field strengths of 2, 1, and 0.5 kV/mm, 1% for electric field strengths of 200 and 100 V/mm, and 10% for electric field strengths of 50, 20, 10, 1, and 0 V/mm. The deformation frequency was varied from 0.01 to 100 rad/s.

Results and discussion

PTAA characterization

The FT-IR spectra of the synthesized PTAA indicated absorption peaks at 2915, 2907, 1703, 1400, 1300–1191, and 835 cm^{-1}, in agreement with the literature. These peaks represent the aliphatic C–H stretch, the in-plane thiophene C–H stretch, the carboxylic acid C = O stretch, the thiophene ring stretch, the carboxylic acid C–O stretch, and the out-of-plane thiophene C–H stretch, respectively [24]. A dominant feature in the spectrum is a broad O–H absorption at wavenumbers in the range 2400–3400 cm^{-1}, which partially obscures the aliphatic C–H stretch peak.

The ^{1}H-NMR spectrum of PTAA in deuterated DMSO reveals absorption peaks at 12.35, 7.27–7.34, and 3.54–3.79 ppm, which can be identified, respectively, as the COOH proton, the thiophene ring protons, and the $–CH_2–$ protons of the thiophene ring [24].

The UV-Vis spectrum of the synthesized PTAA in DMSO shows an absorption peak at 418 nm corresponding to the π–π* transition of undoped PTAA [25]. For $HClO_4$-doped PTAA, the spectrum possesses two dominant peaks at 372 and 475 nm, and a broad peak at 760 nm, which correspond to the π–π* transition of the bipolaron state, the π–π* transition of the polaron state, and the bipolaron transition, respectively [26].

The TGA thermogram of the synthesized PTAA shows two degradation steps at 253 °C and 542 °C corresponding to side chain and backbone degradation, respectively [27].

The mean PTAA particle diameter was determined to be approximately 30 μm with a standard deviation of ~8 μm. The particle microstructure was observed by scanning electron microscopy (SEM). As shown in Fig. 1, the shapes of the undoped and doped PTAA particles are quite irregular, and the particles have a broad size distribution.

The specific conductivity of $HClO_4$-doped PTAA was measured by a custom-built four-point probe. The conductivity increases with dopant concentration, as shown in Table 1. This occurs primarily because of two effects. Increase in dopant concentration causes a corresponding increase in the number of charge carriers, i.e., in the number of polaron and bipolaron species. Also, as the number of charge carriers increases in a PTAA chain, electrostatic repulsion increases the mobility of the charge carriers.

Electrorheological properties of PTAA/silicone systems

The effects of particle concentration and particle conductivity on the ER properties of the suspensions were investigated. The particle concentrations examined were 10 and 20% by weight (corresponding to volume fractions of 0.048 and 0.092, respectively) at a specific conductivity of 7.5×10^{-2} S/cm (HPT10 and HPT20). To study the effect of conductivity, the particle concentration was fixed at 20% by weight and the particle conductivity values were set at 2.0×10^{-4} and 7.5×10^{-2} S/cm for the LPT20 and HPT20 suspensions, respectively. The dynamic moduli, G′ and G″, were measured in the linear viscoelastic regime at a strain of 0.1% for electric field strengths of 2, 1, and 0.5 kV/mm, 1% for electric field strengths of 200 and 100 V/mm, and 10% for electric field strengths of 50, 20, 10, 1, and 0 V/mm as a function of deformation frequency and elapsed time.

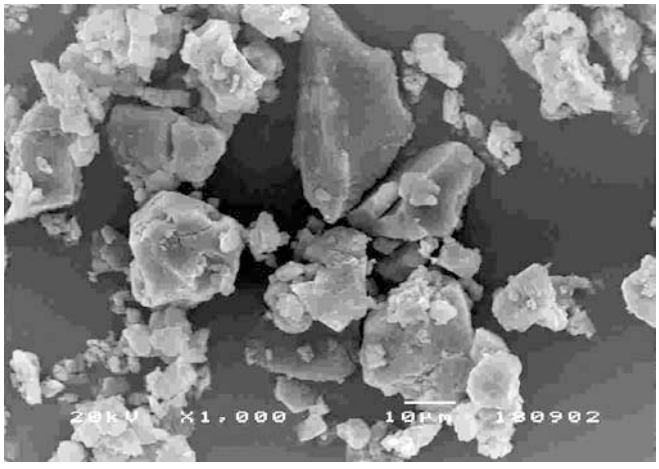

Fig. 1 Scanning electron microscopy of $HClO_4$-doped polythiophene particles

Table 1 Properties of $HClO_4$-doped PTAA suspensions[a] in silicone oil and electrical conductivity values of PTAA pellets[b]

Code	Particle concentration (wt%)	Doping level $[ClO_4]/[S]$	Specific conductivity (S/cm)	Viscosity, η_o (Pa-s)
HPT10	10	0.255	7.5×10^{-2}	0.244
HPT20	20	0.255	7.5×10^{-2}	0.380
LPT20	20	1.09×10^{-3}	2.0×10^{-4}	0.685

[a]Particle size distribution was measured by a particle analyzer whose mean and standard deviation are 30 and 8 μm, respectively
[b]Particle density was 1.97 g/cm^3

Effect of electric field strength

Figures 2a and 2b show that the dynamic moduli $G'(\omega)$ and $G''(\omega)$ of the HPT20 suspension increase dramatically by ten orders of magnitude as the electric field strength is increased through the range 0–2 kV/mm. Close inspection of these results indicates that the system appears to reach a sol-to-gel transition between 50 and 100 V/mm, evidenced by the fact that the storage

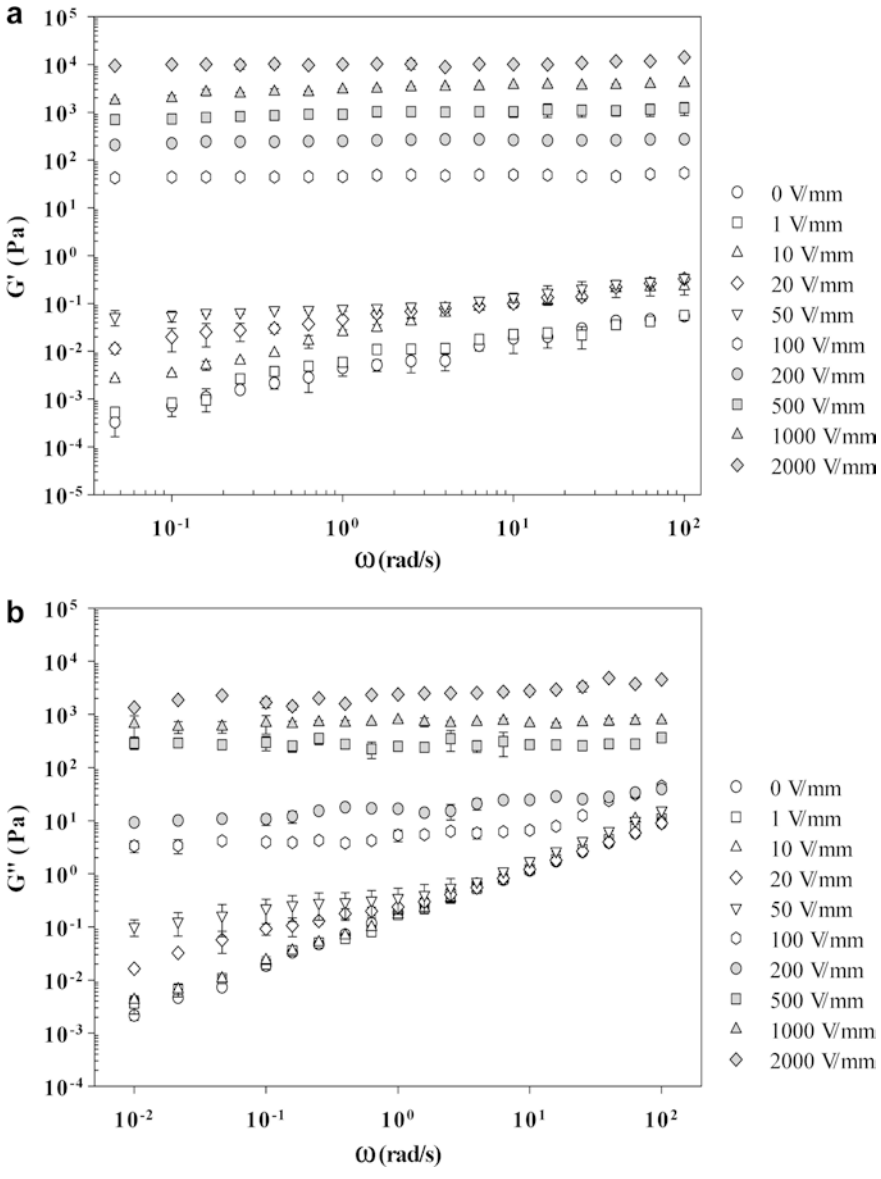

Fig. 2 Storage and loss moduli of 20 wt% highly $HClO_4$-doped polythiophene/silicone oil suspension (HPT20) at 25 ± 0.1 °C: **a** storage moduli G′; **b** loss moduli G″

modulus undergoes a particularly large increase, whereas the loss modulus lags behind. Moreover, at high field strength (1,000 V/mm), G′ and G″ each become essentially frequency independent with G′ larger than G″ ($\tan\delta < 1.0$) at all frequencies. For the HPT10 and LPT20 suspensions, the overall behavior was similar, except that the dynamic moduli were smaller at intermediate field strengths. The increase in the ER response with doping level can be attributed to the enhanced particle polarization due to the increase in particle conductivity [20].

These results are consistent with the generally accepted mechanism for the ER effect in particulate dispersions. Thus, in the absence of the electric field, the particles are randomly dispersed under the influence of the Brownian force. On application of the field, the particles become polarized creating induced dipole moments, leading to interparticle attractions which result in the formation of fibrillar agglomerates in the suspension [16]. Higher field strength induces a higher dipole moment and increases the strength of the interparticle interactions creating longer agglomerates [28]. These longer and stronger agglomerates result in higher rigidity as indicated by a higher G′.

Effect of particle concentration

Figures 3a and 3b compare the G′ and G″ of $HClO_4$-doped PTAA suspensions HPT10 and HPT20 as a

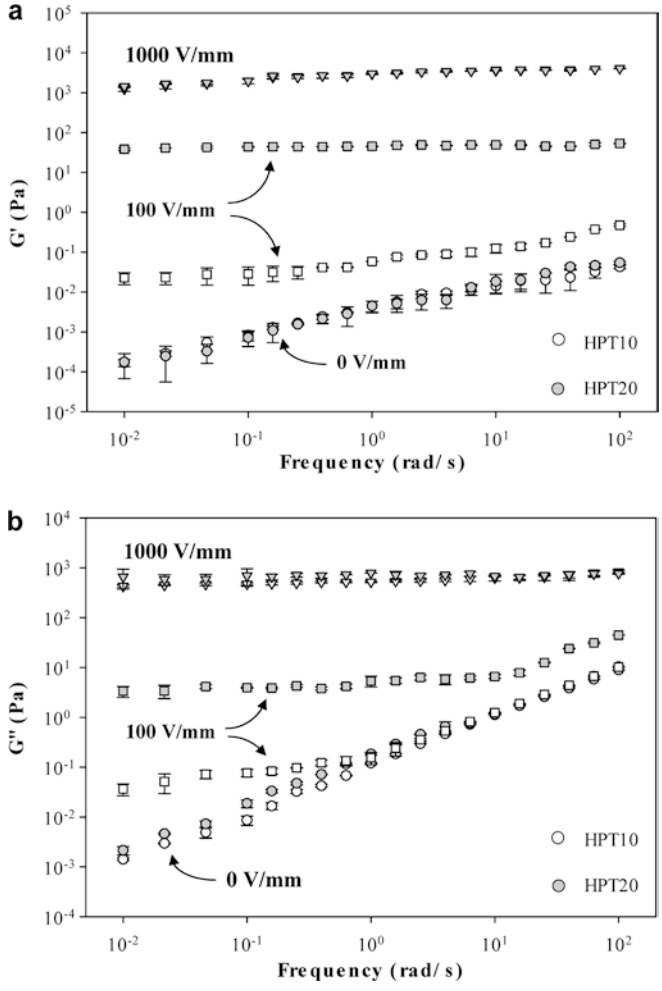

Fig. 3 Storage and loss moduli of highly $HClO_4$-doped polythiophene/silicone oil suspensions at 25 ± 0.1 °C: **a** storage moduli G′; **b** loss moduli G″

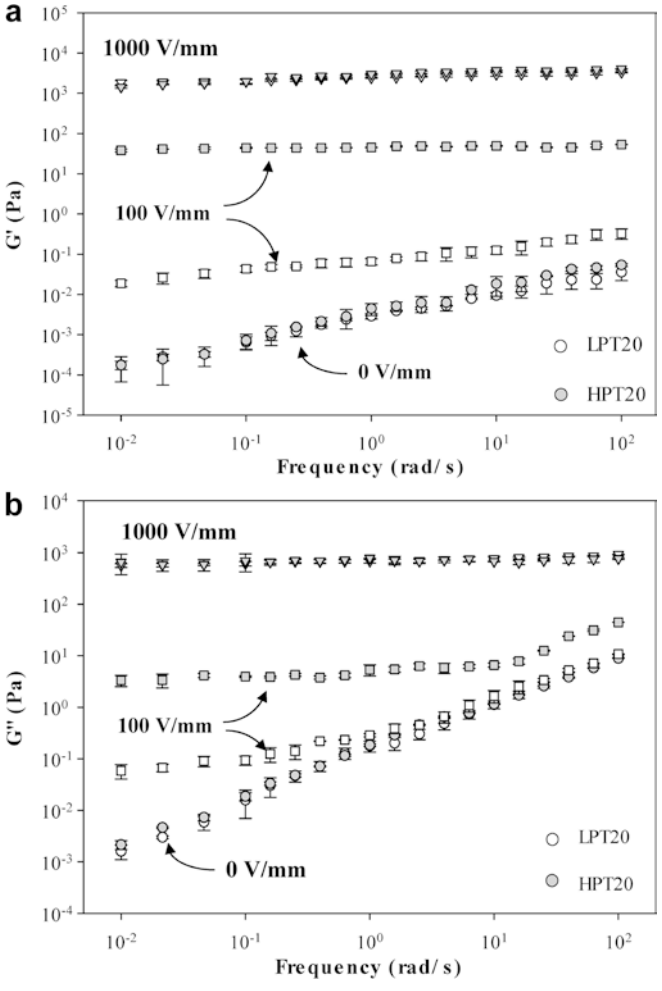

Fig. 4 Storage and loss moduli of 20 wt% $HClO_4$-doped polythiophene/silicone oil suspensions at a temperature of 25 ± 0.1 °C: **a** storage moduli G′; **b** loss moduli G″

function of frequency at field strengths 0, 100, and 1,000 V/mm. In the absence of an electric field, at each concentration, G′ and G″ are of comparable magnitude. The effect of particle concentration becomes apparent at intermediate field strength (100 V/mm), in that the G′ and G″ values of the HPT20 suspension are higher than those of HPT10. The ER properties of the HPT systems appear to saturate at a field strength of 1,000 V/mm, since G′ and G″ are independent of particle concentration. This suggests that, at high field strength and high conductivity, the agglomerate size increases to the point that strong interagglomerate interactions lead to a similar network structure at each concentration. Perhaps, at higher concentration, there are more agglomerates but their sizes are smaller, leading to similar numbers of interagglomerate contacts.

Effect of particle conductivity

Figures 4a and 4b compare the G′ and G″ of $HClO_4$-doped PTAA suspensions LPT20 and HPT20 as a function of frequency at selected field strengths 0, 100, and 1,000 V/mm. The influence of particle conductivity is evident at the intermediate field strength (100 V/mm), in that the G′ and G″ of the HPT20 suspension having higher particle conductivity is substantially larger. The magnitude of the ER effect saturates at the highest field strength of 1,000 V/mm, where the G′ and G″ of LPT20 and HPT20 become comparable in magnitude. Again this leads us to speculate that the high field strength leads to a network structure such that the LPT20 suspension, with lower conductivity, has smaller agglomerates but more of them, resulting in a similar rigidity to that of the HPT20 suspension.

Field-driven sol-to-gel transition

The location of the sol-to-gel transition was investigated as the critical field strength where, at low deformation frequency, G′ becomes larger than G″. In Fig. 5a, G′(0.01) and G″(0.01), the G′ and G″ values at a deformation frequency of 0.01 rad/s, are plotted as a function of the applied field strength for the HPT10 and HPT20 suspensions. Each suspension manifests a sol-to-gel transition, defined at the point where G′(0.01) and G″(0.01) cross over each other. For HPT10 the transition occurs at a higher field strength, 250 V/mm (Fig. 5a), compared to that for HPT20 (60 V/mm). Thus, as expected, a higher particle concentration correlates to a lower field strength for the transition.

In Fig. 5b, G′(0.01) and G″(0.01) are plotted as a function of electric field strength for suspensions LPT20 and HPT20. Again, each suspension shows a transition from fluid-like to solid-like behavior requiring, however, a higher critical field strength of 250 V/mm for the LPT20 suspension having lower particle conductivity.

Time dependence of the ER response

Finally, we investigated the temporal characteristics of the ER response. Figure 6a shows the changes in G′ of HPT20 suspension during a time sweep test, in which an electric field was turned on and off alternately. The temporal response of G′ was recorded in the linear viscoelastic regime at a strain of 0.1% and 1 rad/s frequency under various electric field strengths. On applying the electric field, G′ immediately increases and rapidly reaches a steady-state value. Subsequently, on turning off the field, G′ decreases but does not completely relax to its original value, presumably indicating

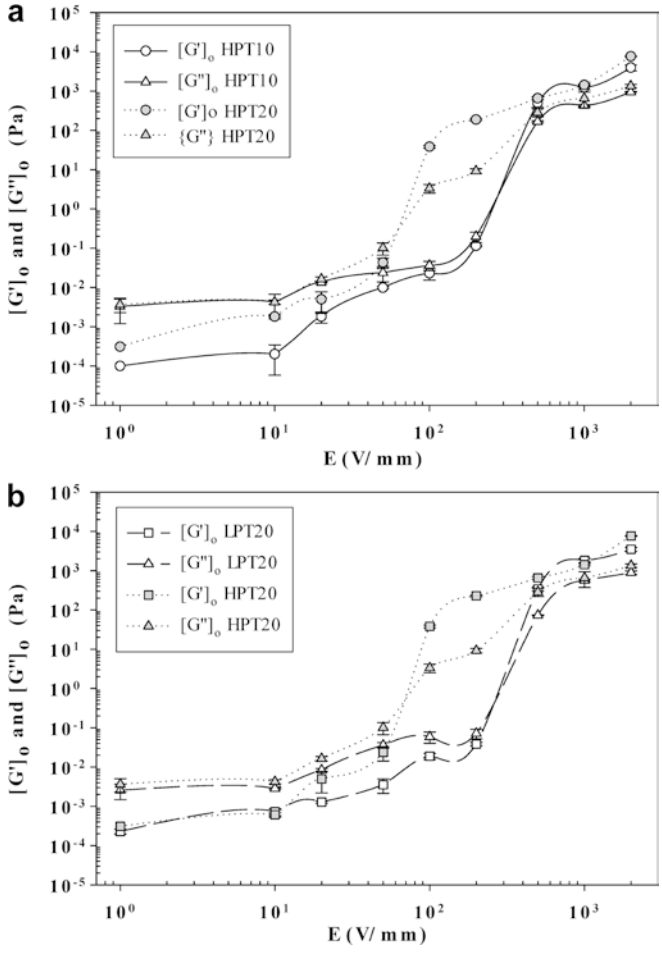

Fig. 5 G′ and G″ values at a deformation frequency $\omega = 0.01$ rad/s of $HClO_4$-doped polythiophene/silicone oil suspensions at a temperature of 25 ± 0.1 °C: **a** highly doped, 10 versus 20 wt% and **b** weakly doped versus highly doped, 20 wt%

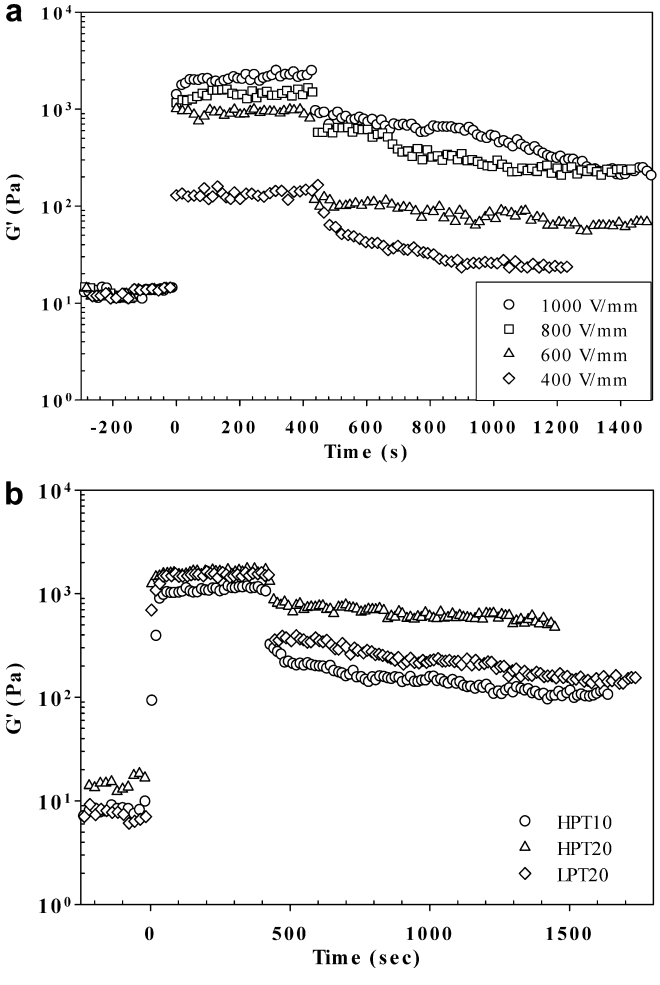

Fig. 6 Temporal response of storage moduli G′ at 25 ± 0.1 °C: **a** 20 wt% highly $HClO_4$-doped polythiophene/silicone oil suspension (HPT20) at various electric field strengths **b** $HClO_4$-doped polythiophene/silicone oil suspensions HPT10, HPT20, and LPT20 are compared at electric field strength 1,000 V/mm

Table 2 Induction and recovery times at 25 ± 0.1 °C of $HClO_4$-doped PTAA suspensions under various electric field strengths

Material	Electric field strength (V/mm)	t_{ind} (s)	t_{rec} (s)
HPT20	100	56	840
	500	55	1180
	800	58	1300
	1000	56	1340
HPT10	1000	54	1275
LPT20	1000	54	1290

some irreversible agglomeration, perhaps due to hydrogen bonding between adjacent particles. As with the field-on modulus, the field-off modulus increases with the applied field strength, indicative that the residual interparticle forces are higher when higher fields have been applied. The time required for G′ to reach the steady-state value on applying the field is called the induction time, t_{ind}, which was found to be essentially independent of the electric field strength, as shown in Table 2. The time required for G′ to reach the steady-state value when the field is turned off is called the recovery time, t_{rec}, which increases with increasing field strength, as shown in Table 2. The independence of t_{ind} from the field strength may reflect that the solvent is passive to the electric field, and hence the particle diffusivity remains unchanged when the field strength is varied. The increase of t_{rec} with the field strength suggests that longer times are required to disperse larger chain-like structures. It is also found that t_{ind} is independent of concentration or conductivity, whereas t_{rec} is longer at lower concentration and lower conductivity (Table 2). Similar behavior to that displayed in Fig. 6a was observed for the HPT10 and LPT20 suspensions on varying the field strength.

Figure 6b compares the G′ responses of doped PTAA suspensions HPT10, HPT20, and LPT20 at a field strength of 1,000 V/mm. It is evident that the field-on values of the modulus vary with concentration and particle conductivity as discussed above. The field-off value of G′ and hence the residual agglomeration also show a dependence on particle concentration and conductivity, being larger at higher concentration and higher conductivity (HPT20 > LPT20 > HPT10).

Scaling analysis

In this section, we carry out a scaling analysis of the ER response of perchloric acid-doped polythiophene suspensions, following the arguments of Parthasarathy and Klingenberg [6]. These authors carried out a dynamic simulation of linear oscillatory shear flow of ER suspensions, treated as hard, neutrally buoyant, uncharged dielectric spheres immersed in a dielectric, Newtonian continuous fluid. Application of an electric field polarizes the spheres, with electrostatic interaction between them, and between each sphere and the electrodes. For large particles under large electric fields, colloidal and Brownian forces can be neglected. The equation of motion for particles, neglecting hydrodynamic interactions, can be written as

$$\frac{d\mathrm{r_i}}{d\mathrm{t}} = \mathrm{u}^{\infty}(\mathrm{r_i}) + \frac{1}{3\pi\eta_c \mathrm{d}}\left[\mathrm{F_i^{el}} + \mathrm{F_i^{rep}}\right]$$

where r_i is the center position of particle i, $u^{\infty}(r_i)$ is the ambient fluid velocity evaluated at the particle center, η_c is the viscosity of the continuous phase, d is the particle diameter, F_i^{el} is the electrostatic force between particle i and other particles, and F_i^{rep} is the short-range repulsion between particle i and other particles and between particle i and the electrodes.

The ensemble-averaged electrostatic force exerted on a particle i by particle j in the point-dipole limit is given by

$$\left\langle \mathrm{F_{ij}^{el}} \right\rangle = \mathrm{F_s}\left(\frac{\mathrm{d}}{\mathrm{r_{ij}}}\right)^4 \left[\left(3\cos^2\theta_{ij} - 1\right)\right] \mathrm{e_r} + \sin 2\theta_{ij}\mathrm{e}_{\theta}$$

where

$$\mathrm{F_s} = \frac{3}{16}\pi\varepsilon_o\varepsilon_c \mathrm{d}^2 \mathrm{E_{rms}^2}\left(\beta^*\bar{\beta}^*\right)$$

where r_{ij} is the distance between particle i, which locates at the origin of a spherical coordinate system, and particle j, θ_{ij} is the angle between the e_z axis and r_{ij}, $\varepsilon_o = 8.8542\times10^{-12}$ F/m, $\beta^* = (\varepsilon^*_p - \varepsilon^*_c)/(\varepsilon^*_p + 2\varepsilon^*_c)$, the subscript p refers to the particle and the subscript c refers to the continuous medium. $\varepsilon^* = \varepsilon - j\sigma/\varepsilon_o\omega_E$ is the complex dielectric constant, where ε is the relative dielectric constant, σ is the specific conductivity, and ω_E is the angular frequency of the applied electric field, $E = E_o e^{j\omega_E t} e_z$. $E_{rms} = E_o/\sqrt{2}$ and β^* is the complex conjugate of β^*. In the low-frequency limit ($\omega_E \to 0$), the force scales as

$$\mathrm{F_s} = \frac{3}{16}\pi\varepsilon_o\varepsilon_c \mathrm{d}^2 \mathrm{E_{rms}^2}\left(\frac{\sigma_p - \sigma_c}{\sigma_p + 2\sigma_c}\right)^2$$

and in the high-frequency limit ($\omega_E \to \infty$), the force scales as

$$\mathrm{F_s} = \frac{3}{16}\pi\varepsilon_o\varepsilon_c \mathrm{d}^2 \mathrm{E_{rms}^2}\left(\frac{\varepsilon_p - \varepsilon_c}{\varepsilon_p + 2\varepsilon_c}\right)^2$$

The short-range repulsive force between spheres is represented by

$$\mathrm{F_{ij}^{rep}}(\mathrm{r_{ij}}) = -\mathrm{F_s}\exp\left(-\mathrm{K}\frac{\mathrm{r_{ij}} - \mathrm{d}}{\mathrm{d}}\right)\mathrm{e_r}$$

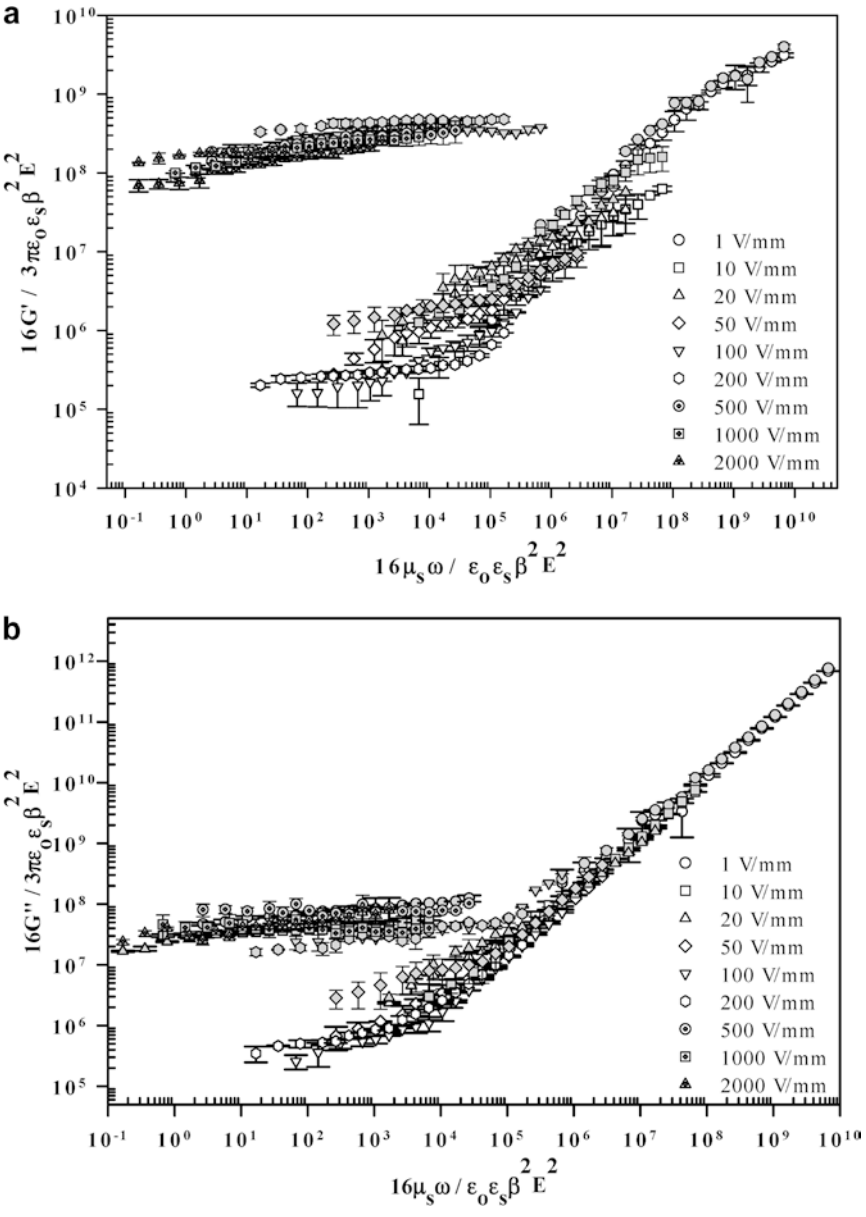

Fig. 7 Master plot superposing G′ and G″ data of $HClO_4$-doped polythiophene/silicone oil suspensions at 25 ± 0.1 °C: **a** storage moduli G′; **b** loss moduli G″. *Open symbols* represent LPT20 and *solid symbols* represent HPT20**.** Here, $\varepsilon_o = 8.8542\times10^{-2}$ F/m, ε_s 2.71 F/m, $\mu_s = 10^{-4}$ m^2/s, and $\beta = 0.9985$ and 0.9999 for LPT20 and HPT20, respectively

where K is a dimensionless parameter characterizing the magnitude of the repulsive potential.

The sphere/wall interaction is represented by a similar short-range function,

$$F^{rep}_{i,wall}(r_i) = -F_s \exp\left(-K\frac{h_i - d/2}{d}\right) n$$

where $h_i = L_z/2 - z_i$, L_z is the electrode gap width, z_i is the distance between particle i and electrode, and n is the unit normal vector directed from the electrode into the suspension.

The equation of motion can be made dimensionless with the following length, force, and time scales:

$$\ell_{sc} = d, \quad F_{sc} = \frac{3}{16}\pi\varepsilon_o\varepsilon_c d^2\beta^2 E^2_{rms}, \quad t_{sc} = \frac{16\eta_c}{\varepsilon_o\varepsilon_c\beta^2 E^2_{rms}}$$

where

$$\beta^2 \equiv \beta^*\bar{\beta}^*.$$

The equation of motion in dimensionless variables can therefore be written as

$$3\pi\eta_s d \cdot \frac{u_{sc}}{F_{sc}}\left[\frac{dr_i'(t)}{dt'} - u'(x', t')\right] = F_i'^{el}$$

It follows that the dimensionless rheological responses must be functions of only the dimensionless frequency [28]:

$$\frac{G'}{(3/16)\pi\varepsilon_o\varepsilon_c\beta^2E_o^2} = f_1\left(\frac{16\eta_c\omega}{\varepsilon_o\varepsilon_c\beta^2E_o^2}\right)$$

$$\frac{G''}{(3/16)\pi\varepsilon_o\varepsilon_c\beta^2E_o^2} = f_2\left(\frac{16\eta_c\omega}{\varepsilon_o\varepsilon_c\beta^2E_o^2}\right)$$

Figures 7a and 7b show the master plots for G′ and G″, respectively, obtained by superposing the corresponding data from 20 wt% $HClO_4$-doped PTAA/silicone oil suspensions of high and low conductivities (HPT20 and LPT20). It is evident that the scaled values of the storage and loss moduli for these PTAA suspensions at various electric field strengths and frequencies approximately collapse onto a single function of the dimensionless frequency, indicating a moderate success of the model of Parathasarathy and Klingenberg [28].

Conclusion

In the present study, poly(3-thiopheneacetic acid) particles were synthesized via an oxidative polymerization and doped with perchloric acid. The ER properties of the $HClO_4$-doped PTAA/silicone oil suspensions were then investigated by examining the effects of electric field strength, particle concentration, and particle conductivity on the dynamic moduli, G′ and G″. The results show that G′ and G″ increase dramatically by ten orders of magnitude when the electric field strength is increased to 2 kV/mm. Furthermore, the PTAA-based ER fluids exhibited highly viscoelastic behavior under an applied electric field due to the formation of agglomerates induced by the electric polarization within particles. The ER response is enhanced by increasing the electric field strength, the particle concentration, and the particle conductivity. The PTAA suspensions exhibit a transition from fluid-like to solid-like behavior as the field strength is increased. The influence of particle concentration and particle conductivity is most apparent at intermediate field strengths, and the suspensions show a saturation in ER properties at a field strength of 1 kV/mm. This suggests a change in the nature of the agglomerate structure at high field strengths and high conductivity and/or concentration, such as network formation. Finally, the frequency-dependent moduli at different electric field strengths and conductivities, when scaled according to the model of Parathasarathy and Klingenberg [28], moderately collapse into single functions of the dimensionless frequency. Of course the latter treatment may be expected to fail under conditions where interagglomerate interactions become important, i.e., in the saturation regime.

Acknowledgements The authors would like to acknowledge the financial support provided by The Thailand Research Fund (TRF) in the RGJ grant no. PHD/0128/2542 and TRF-BGJ grant no. BGJ/03/2544.

References

1. Sakurai R, See H, Saito T, Asai S, Sumita M (1999) Rheol Acta 38:478
2. Voyles RM, Fedder G, Khosla PK (1996) Proceedings of the 1996 IEEE international conference on robotics and automation
3. Kamath GM, Wereley N (1997) Smart Mater Struct 6:351
4. Pfeiffer C, Mavroidis C, Cohen YB, Dolgin B (1999) Proceedings of the 1999 SPIE telemanipulator and telepresence technologies VI conference
5. Fees G (2001) Olhydraul Pneumat 45:1
6. Parthasarathy M, Klingenberg DJ (1999) J Non-Newtonian Fluid Mech 81:83
7. Chin BD, Winter HH (2002) Rheol Acta 41:265
8. Ha JW, Yang SM (2000) J Rheol 44(2):235
9. McLeish TCB, Jordan T, Shaw MT (1991) J Rheol 35(3):427
10. Jordan TC, Shaw MT, McLeish TCB (1992) J Rheol 36(3):441
11. Jang WH, Kim JW, Choi HJ, Jhon MS (2001) Colloid Polym Sci 279:823
12. Kim SG, Kim JW, Choi HJ, Suh MS, Shin MJ, Jhon MS (2000) Colloid Polym Sci 278:894
13. Lee JH, Cho MS, Choi HJ, John MS (1999) Colloid Polym Sci 277:73
14. Krause S, Katherine B (2001) Macromolecules 34:7179
15. Lee HJ, Chin BD, Yang SM, Park OO (1998) J Colloid Interface Sci 206:424
16. Lee YH, Kim CA, Jang WH, Choi HJ, Jhon MS (2001) Polymer 42:8277
17. Cho MS, Kim JW, Choi HJ, Webber RM, Jhon MS (2000) Colloid Polym Sci 278:61
18. Jun JB, Lee CH, Kim JW, Suh KD (2002) Colloid Polym Sci 280:744
19. Choi HJ, Cho MS, Kim JW (2001) Korea-Australia Rheol J 13(4):197
20. Kim YD, Park DH (2002) Colloid Polym Sci 280:828
21. Goodwin JW, Markham GM, Vincent B (1997) J Phys Chem 101:1961
22. Cho MS, Choi HJ (2000) Korea-Australia Rheol J 12(3/4):151
23. Sim IS, Kim JW, Choi HJ (2001) Chem Mater 13:1243
24. Kim B, Chen L, Gong J, Osada Y (1999) Macromolecules 32:3964
25. Chen L, Kim B, Nishino M, Gong J, Osada Y (2000) Macromolecules 33:1232
26. Demanze H (1996) Macromolecules 29:4267
27. Radcliffe CJ, Lloyd JR, Andersland RM, Hargrove JB (1996) Proceedings of the ASME international congress and exhibition
28. Parthasarathy M, Ahn KH, Klingenberg DJ (1994) Int J Mod Phys B 8:2789